Cone-Beam CT Systems

2

Jeffrey H. Siewerdsen

Basic Principles of Cone-Beam CT

Introduction

Many works have reviewed aspects of cone-beam CT (CBCT). Basic principles are covered in textbooks by Hsieh [1], Buzug [2], Shaw [3], Brock [4], and Zhou [5]. In the following short subsections of the Introduction, we touch on the key principles and considerations of CBCT and provide references to previous sources that treat each topic in depth. The main bulk of this chapter is treated in Sect. 2, which aims to elucidate the distinctions (and commonalities) of CBCT with respect to multi-detector CT (MDCT).

Physical Configurations

The diversity of physical platforms for CBCT and their corresponding clinical applications are described by Siewerdsen and Schafer [5]. These include C-arm [6], U-arm [7], and O-arm [8] gantries and applications ranging from image-guided interventions (e.g., surgery [9], interventional radiology [10], cardiac interventions [11], and radiation therapy [7]) to diagnostic specialties (e.g., dental [12], ENT [13], breast [14], and orthopedics [15]).

J. H. Siewerdsen (✉)
Department of Biomedical Engineering,
Johns Hopkins University, Baltimore, MD, USA
e-mail: jeff.siewerdsen@jhu.edu

Image Reconstruction

Methods and algorithms for CBCT image reconstruction are described in the textbooks by Hsieh [1] and Buzug [2]. The first practical, analytical algorithm for CBCT image reconstruction is commonly identified as the Feldkamp-Davis-Kress (FDK) algorithm [16]. Many variations on the FDK algorithm have emerged, but its basic principles – e.g., the cosine weighting associated with the density of rays incident on a 2D flat detector – remain the workhorse underlying algorithm for many CBCT systems. We will retread neither the analytical form nor its common algorithmic implementations here – except perhaps to add one note: CBCT system developers might consider generalization of the (1D) smoothing/apodization filter implemented to counter high-frequency ramp-filtered noise into a more symmetric 2D form (i.e., acting on both rows and columns of the detector) in the interest of more isotropic spatial resolution characteristics in the resulting 3D image reconstruction – as noted in the paper by Uneri et al. [17].

Model-based image reconstruction (MBIR) methods involving iterative optimization represent a major area of research in CBCT – offering potential benefits in image quality and dose reduction compared to FBP. Review of such methods in CBCT can be found in [4] and [18]. As with FBP, will we not retread mathematics or broad range of algorithms associated with MBIR in CBCT – nor the emerging space of deep learning approaches for 3D image reconstruction – except

E. Samei, N. J. Pelc (eds.), *Computed Tomography*, https://doi.org/10.1007/978-3-030-26957-9_2

perhaps to echo the sentiments underlying the work of Stayman et al. [19–21] that CBCT systems with flat-panel detectors (FPDs) and diverse source-detector orbits (e.g., noncircular orbits on a robotic C-arm) may benefit even more from MBIR than their counterparts in MDCT, which tend to feature highly optimized detectors and circular acquisition geometry; therefore, the relative benefits of MBIR may be even greater for FPD-CBCT systems.

Image Quality

The factors affecting CBCT image quality have been described in sources such as [3] and [9]. Among the most important factors are

- Characteristics associated with the detector (e.g., blur, lag, and electronic noise);
- Effects associated with the elevated levels of x-ray scatter in a broad volumetric beam (e.g., reduction of image uniformity and contrast); and
- Susceptibility to patient motion artifacts during the long (5–60 s) scan time for CBCT. Each of these areas presents important challenges motivating ongoing research

Applications

The first clinical applications of CBCT were in two very different areas. By 2000–2001, CBCT began to emerge in a variety of systems for dental imaging, as reviewed by Pauwels et al. [12]. Concurrently, CBCT for image-guided radiotherapy was developed via research led by Jaffray et al. [7]. Development of CBCT capability with fixed-room (floor- or ceiling-mounted) C-arms for 3D angiography [10] progressed rapidly from platforms based on x-ray image intensifiers (XRIIs), with FPD-CBCT C-arms becoming commonplace in interventional radiology by 2010. CBCT on mobile C-arms progressed similarly from XRII systems (e.g., the Siemens Iso-C 3D [22]) to higher-quality systems incorporating a FPD [6] and emerging in image-guided surgery on systems by Medtronic [23], Ziehm [24], and Siemens [25]. In the last decade, a number of specialty diagnostic imaging systems based on CBCT have emerged for applications beyond dental imaging. These include breast CBCT as developed by Boone et al. [14] and Ning et al. [26] and systems for musculoskeletal/orthopedic imaging [15] as evident in the Carestream Onsight 3D, Planmed Verity, and CurveBeam PedCat systems.

Overview of This Chapter

With the very brief overview of CBCT characteristics and systems provided above, the remainder of this chapter attempts to survey and clarify the distinctions and commonalities of CBCT and MDCT. For more in-depth description of algorithms, hardware, and applications, the reader is referred to the various sources mentioned above.

In the following section, we survey numerous important aspects of CBCT compared and contrasted to MDCT – the latter representing the state-of-the-art in CT imaging for diagnostic radiology. Commonalities and distinctions between CBCT and MDCT are delineated, and the considerable gray area between the two is brought somewhat into focus. As we will see, even the name associated with the technology – "cone beam" – is ambiguous and incomplete (and, in fact, incorrect) in distinguishing CBCT from MDCT. With an appreciation of the numerous factors surveyed below, it is hoped that the reader interested in CBCT – be that the physics, algorithms, dosimetry, applications, or even regulatory considerations – will be somewhat clearer, and even if a definitive distinction is not reached, the reader will at least be better able to "know it when she/he sees it" and form an educated perspective on these modalities.

Cone-Beam CT Systems

An accurate assertion: *CBCT is MDCT*. By that, we simply say that a CBCT system employs a detector with multiple rows.

An equally accurate converse: *MDCT is CBCT*. By that, we simply say that a MDCT system involves a volumetric x-ray beam with appreciable extent in the longitudinal direction.

What then – if anything – is the difference? Read on.

Genesis

A variety of CBCT systems began to emerge in the early 2000s for applications ranging from image-guided radiation therapy (IGRT) [27] and 3D angiography [28] to dental/ENT [29] and breast imaging [26]. Such developments were coincident with the independent emergence of MDCT also in the early 2000s [30], igniting the "Slice Wars" among 4-, 8-, 16-, 32-, 64-, 256-, and 320-slice scanners for diagnostic radiology and cardiology. The genesis of these two technologies was simultaneous and independent: CBCT was for the most part born to smaller scale efforts in a diversity of clinical specialty applications via academic research and entrepreneurial startup companies; meanwhile, MDCT was propelled primarily by major industry concerns (e.g., GE, Philips, Siemens, and Toshiba) sparking a revolution in diagnostic CT that advanced the modality beyond its conventional "axial mode" (single-slice) acquisition to enable faster scanning with more isotropic spatial resolution [31].

System Geometry and the (Inaccurately Named) "Cone" Beam

CBCT and MDCT systems share a variety of characteristics in system geometry – e.g., an x-ray beam divergent in and covering an appreciable extent in the longitudinal (z) direction. In this respect, it is difficult to specify a unique definition of what constitutes a "cone-beam" system, since both CBCT and MDCT systems share this aspect of broad-beam geometry. In fact, given the rectangular (vs. circular) format of the detector, "pyramid" beam is a more precise designation than "cone" beam. The basic system geometry for CBCT and MDCT is illustrated in Fig. 2.1, and Table 2.1 lists a number of characteristics of MDCT and CBCT systems, including aspects of the x-ray source, detector, image acquisition, etc. - and considerable areas of overlap between the two.

The X-Ray Source

With some exceptions (e.g., breast CBCT), both CBCT and MDCT systems tend to operate in a similar range of the diagnostic x-ray spectrum – ~80–120 kV. One typical distinction, however, is that CBCT systems tend to be implemented with a pulsed radiographic/fluoroscopic x-ray tube (with fairly limited heat capacity, pulsing at a rate up to ~30 pulses/s consistent with FPD readout rate). MDCT systems, on the other hand, are typified by continuous x-ray exposure (continuous mA) with high-performance x-ray tubes featuring high heat capacity.

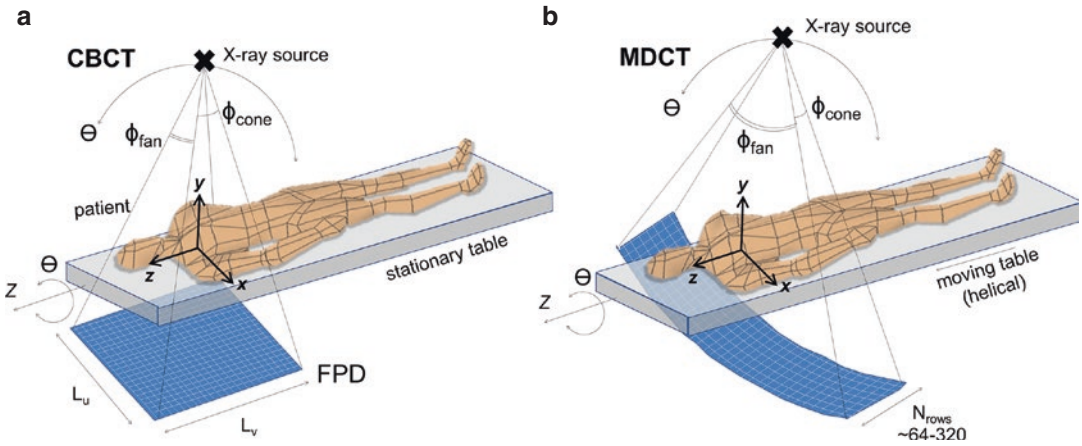

Fig. 2.1 Illustration of cone-beam system geometry. (**a**) CBCT with a flat detector. (**b**) MDCT with a curved detector. (Illustration by Nicole Chernavsky, Johns Hopkins University)

Table 2.1 Characteristics of volumetric x-ray tomography systems, with example (typical) descriptions for MDCT and CBCT systems

	Multi-detector CT (MDCT)	Cone-beam CT (CBCT)
X-ray source	High power (100–240 kW)	Lower power (3–100 kW)
	Continuous mA	Pulsed mA
Detector	64 rows (up to 320 rows)	>1024–2048 rows
	~few cm z coverage (up to 16 cm)	>20 cm z coverage
Acquisition speed	Fast (~3–5 rotations/s)	Slow (~1 rotation in 5–60 s)
	1000s of projections/rotation	100 s of projections/rotation
Orbit	Circular/helical	Circular (semicircular) or
	Fast table feed (>10–50 cm/s)	Noncircular (e.g., dual isocenter)
Image quality	Excellent bone + soft-tissue visualization	Good bone visualization
	Contrast-enhanced scan protocols	Isotropic spatial resolution
	Spectral/dual-energy capability	Modest soft-tissue contrast resolution
		Strong artifacts (scatter and motion)
Applications	Diagnostic radiology (specialty interventional systems)	Image-guided interventions (specialty diagnostic systems)

Each modality is capable of beam modulation (i.e., variation of kV and/or mA), but CBCT systems tend to incorporate such capability only in relation to the automatic exposure control of the detector (to provide a sufficient level of exposure to the detector while avoiding sensor saturation), whereas MDCT systems employ a variety of dedicated modulation schemes designed to reduce dose to the patient.

Multi-source CBCT and MDCT systems present interesting variations within each technology. In CBCT, a distribution of x-ray sources along the z axis has been shown to extend the longitudinal FOVz and reduce cone-beam artifacts [33]. In MDCT, incorporation of two x-ray tubes (and detectors) on the gantry typified the "dual-source" scanner introduced by Siemens primarily to increase temporal resolution, also permitting dual-energy MDCT [34].

The Detector

Among the characteristics that tend to distinguish CBCT and MDCT systems is the x-ray detector. As illustrated in Fig. 2.1, CBCT systems are typified by a flat detector – for example, a flat-panel detector (FPD) formed of CMOS or a-Si:H active matrix readout [25]. By contrast, MDCT systems incorporate a curved detector formed of highly optimized banks of multi-row detector modules, with a diversity of semiconductor and scintillator architectures.

Key differences in detector characteristics and performance include the following:

- For FPDs in CBCT: flat detector format, higher spatial resolution (smaller pixels), multi-mode fluoroscopy/radiography/CBCT imaging, and relatively lower cost
- For MDCT detectors: curved detector format, higher detective quantum efficiency, lower electronic noise, higher frame rate, and deeper bit depth

The distinction in flat or curved detector formats also carries a distinction in weighting factors involved in 3D filtered backprojection (FBP), as described in the textbook by Hsieh [1].

Post-Patient Collimator/Anti-scatter Grid

A broad volumetric beam is associated with high levels of x-ray scatter [35], so scatter rejection (and correction) is an important factor in the uniformity, contrast, noise, and artifact in both CBCT and (esp. 256- or 320-slice) MDCT systems. Post-patient collimation on CBCT systems typically involves a simple anti-scatter grid (usually linear) – if a grid is used at all [36, 37]. The selec-

tion of optimal grid (or gridless) configuration is an area of research within CBCT system development, usually concluding that compact CBCT systems with a very short axis-detector distance (small air gap) benefit from the use of a grid, but systems with large air gap may or may not benefit from incorporation of a grid [38]. MDCT systems, on the other hand, employ a highly optimized 2D post-patient collimation grid.

Field of View (FOV)

CBCT systems with a FPD tend to have fairly small lateral FOV, and lateral truncation (of the patient and/or table) is the norm. As illustrated in Fig. 2.1, FPDs have lateral extent (L_u) up to ~41 cm, giving axial FOV (FOV_{xy}) of ~20–25 cm, depending on system magnification. An offset detector geometry (i.e., displacing the detector laterally by up to half its width) and acquisition of projections over a full 360° orbit effectively expands FOV_{xy} to ~(40 × 40) cm^2 at the cost of sampling density and acquisition speed. A sliding or dual-isocenter approach accomplishes an analogous increase in FOV_{xy} for C-arm CBCT systems.

The FOV_{xy} for MDCT is comparatively large and typically avoids lateral truncation of the patient and table (excepting very obese subjects). An MDCT detector has lateral extent sufficient to cover FOV_{xy} ~(50 × 50) cm^2.

Table Motion

CBCT systems typically involve no table motion – i.e., the patient table is fixed, and the source and detector move in an orbit about the patient to acquire a volumetric image. Conversely, MDCT systems typically involve helical motion – i.e., longitudinal motion of the table. In some MDCT implementations (e.g., the Brainlab Airo and BodyTom), helical acquisition is accomplished via longitudinal motion of the gantry [39, 40].

Although algorithms for 3D image reconstruction in "helical CBCT" are tractable (e.g., Katsevich [41]), CBCT systems are not usually implemented for helical scanning (i.e., longitudinal motion of the patient during the scan). Rather, CBCT systems typically operate with the patient stationary on the table, and the source-detector system rotates once to acquire the volumetric image. This is advantageous in requiring only motion of the source-detector gantry (e.g., C-arm, U-arm, or O-arm gantries) and therefore carrying a comparatively simpler system configuration. It is also advantageous in clinical applications involving a complex patient setup and diversity of other systems about the patient – e.g., in surgery.

MDCT, on the other hand, is typified by helical acquisition – with exquisitely engineered tables for longitudinal translation of the patient during the scan. Even 320-slice systems will typically "cone down" to 64-slice coverage plus helical motion to acquire long volumetric scans. The volumetric 320-slice mode is used primarily for whole-organ scanning of the heart, brain, or liver.

Scan Speed

CBCT systems are typically slow. CBCT C-arms rotate up to 45 °/s, with minimum scan time around 5 s. Systems with 15, 30, or 60 s scan time are common. Such long scan times introduce strong susceptibility to artifacts arising from patient motion, as described below. With FPD readout up to ~30 fps, the number of projections acquired in a CBCT scan tends to be fairly low (~200–600 views) compared to MDCT (>1800 views).

MDCT, on the other hand, is typified by fast gantry rotation ~0.2–0.3 s per revolution – more than an order of magnitude increase in speed (per rotation) compared to CBCT. Temporal resolution down to 18–30 ms permits visualization of the beating heart, as discussed below. Susceptibility to patient motion artifacts is correspondingly low, even for helical acquisition covering an extended length of the patient, since motion-related data inconsistencies are mostly limited to the rotation interval (~0.2–0.3 s) rather than the total scan time.

The Imaging Platform and Scan Trajectory

CBCT imaging systems are often implemented in a fairly open geometry, such as a C-arm gantry or mounted on the face of a radiotherapy linac. Accordingly, CBCT systems may enjoy flexibility in scan trajectory – e.g., offset detector geometry to expand the lateral FOV; dual-isocenter (Zeego); noncircular orbit on non-isocentric C-arm (Ziehm); or noncircular orbits designed to improve sampling/image quality (Zeego task-driven orbits).

MDCT systems are typically within a closed ring gantry limited to circular (helical) orbit – the iconic donut that typifies scanners in diagnostic radiology.

Power

The power of the generator is another typical distinction between CBCT and MDCT systems. The former tend to be lower power – e.g., 3–10 kW mobile systems and up to ~200 kW fixed-room C-arm systems. The latter carry the potential for considerably higher power – e.g., up to 240 kW.

Portability

The relative simplicity and flexibility of CBCT systems is reflected in their implementation in numerous mobile systems – e.g., Ziehm, Medtronic, Siemens, Carestream Onsight, etc. That said, many fixed-room implementations exist for CBCT as well – e.g., IGRT and ceiling- or floor-mounted 3D angiography systems.

MDCT systems are typified by dedicated site installation fixed within a shielded room – the backbone of diagnostic CT in radiology. Fixed-room installation is common for MDCT, but not exclusive, and a variety of mobile MDCT systems have also been introduced – e.g., Brainlab Airo, Philips Tomoscan, and Samsung BodyTom and CereTom.

Imaging Modes

Many CBCT systems are capable of acquiring not only 3D volumetric images but also 2D radiographic or fluoroscopic images – or even tomosynthesis imaging (i.e., limited-angle CBCT) [42]. For example, mobile C-arms for image-guided surgery permit "spot-film" or fluoroscopic imaging capability, with 3D images typically acquired infrequently – e.g., at the beginning of the case for purposes of planning, at a milestone during the case to check the integrity of surgical product, or at the end of the case to validate surgical product and/or check for possible complications.

MDCT systems typically do not permit 2D fluoroscopic imaging (i.e., real-time continuous capture of a large-area 2D projection image). Rather, MDCT systems may allow "CT Fluoro" acquisition in which the patient couch is stationary, the source-detector continuously rotates within the slip-ring gantry, and axial slices (covering a relatively narrow longitudinal extent) are acquired in near real-time.

4D Imaging

4D imaging capability (i.e., a time series of 3D volumetric images) is possible in various forms for both CBCT and MDCT systems. The latter are capable of true real-time 4D imaging – i.e., acquisition of fully 3D data at acquisition rates less than 1 s, e.g., 4D MDCT of the heart with volumetric images covering 16 cm longitudinal extent acquired at real-time sampling rates up to ~5 volumes per second.

Other variations of 4D imaging can be found on both CBCT and MDCT systems. Two forms of gated acquisition (prospective and retrospective) work as follows. Prospectively gated acquisition triggers the acquisition of projection data at a particular desired phase of motion (e.g., ECG gating to trigger during diastole), providing 3D imaging of a dynamic scene with reduced motion artifact. Retrospectively gated imaging involves acquisition of projection data throughout all phases of motion and retrospective sorting of the projection data to allow 3D

image reconstruction at any particular phase and/or all phases. The latter constitutes a form of 4D imaging, recognizing the difference between true real-time 4D imaging (brute force high-speed real-time volumetric data capture) and retrospectively phase-binned 4D imaging (according to monitoring of some – hopefully periodic – motion signal) to provide a 4D facsimile of (periodic) motion.

Imaging Performance: Spatial Resolution

By virtue of fairly fine pixel spacing of FPDs (typically 0.15–0.4 mm square pixels), CBCT enjoys fairly high spatial resolution in 3D image reconstructions. For FPD readout modes with isotropic pixel binning (1 × 1, 2 × 2, etc.), the spatial resolution in CBCT reconstructions can be similarly isotropic – recognizing that the choice of apodization filter [17] or other post-processing can impose non-isotropic resolution. Depending on the scan protocol and reconstruction method, CBCT images typically provide isotropic spatial resolution with a limiting resolution of ~1–2 lp/mm (minimum feature size ~0.5 mm).

MDCT systems (and certainly conventional single-slice axial CT scanners) conventionally exhibited somewhat coarser spatial resolution than CBCT, but newer detector technologies and scan protocols for MDCT have begun to erase the deficit. Depending on scan protocol and reconstruction method, MDCT systems may provide spatial resolution with limiting resolution ~0.5–1 lp/mm (minimum feature size ~0.65 mm). Emerging MDCT scanner designs push resolution limits further by incorporation of still higher-resolution detectors, for example Canon Precision CT. Higher spatial resolution can be achieved by adjustment of the scan protocol (e.g., fine helical pitch, with a proportional penalty in dose) and application of a sharp apodization filter – e.g., temporal bone scan protocols. The degree to which MDCT reconstructions are isotropic depends on the choice of helical pitch, voxel size (and slice thickness), and reconstruction method.

Imaging Performance: Contrast and Noise

Owing primarily to high levels of x-ray scatter and suboptimal post-patient collimation (antiscatter grid, or gridless operation), CBCT systems typically exhibit lower subject contrast than MDCT. As a result, soft-tissue imaging capability presents a challenge to CBCT.

Contributing to the challenge are factors of x-ray scatter, lower DQE (quantum detection efficiency ~0.65), a relatively high level of electronic noise, and low digitization bit depth of FPDs for CBCT compared to higher performance detector systems in MDCT. This tends to result in reduced contrast resolution (e.g., contrast-to-noise ratio) for CBCT systems. Many CBCT systems are sufficient only for bone (and metal device) visualization, and soft-tissue contrast resolution is relatively poor.

Improving the soft-tissue contrast resolution of CBCT has presented an important area of ongoing research. For example, the application of MBIR to C-arm and O-arm CBCT systems for image-guided surgery has been shown to enhance soft-tissue visualization in support of soft-tissue surgeries and to provide a check on complications [17, 43]. Similarly, optimal system design was shown to provide reasonable levels of visibility of cartilage, ligament, and tendons in CBCT of the extremities [44]. A particular challenge of contrast resolution was demonstrated in the development of CBCT systems for imaging of acute stage intracranial hemorrhage, where a combination of optimal system design, protocol selection, artifact correction, and MBIR was shown to advance CBCT image quality to a level sufficient for visualization of intracranial hemorrhage [32, 45–48].

MDCT, on the other hand, enjoys a level of contrast resolution suitable to a broad range of low-contrast, soft-tissue anatomy in the brain, abdomen, and pelvis. Such capability has positioned MDCT as the front line for diagnosis for many indications, including detection or rule out of hemorrhage in emergency settings.

Imaging Performance: Artifacts Associated with the X-Ray Beam

As noted above, CBCT and MDCT systems tend to operate in a similar range of diagnostic energies (~80–120 kV) and are therefore susceptible to similar biases associated with the x-ray beam. X-ray scatter and beam hardening are two such effects, leading to shading and streak artifacts in CBCT or MDCT reconstructions.

X-ray scatter increases steeply as the longitudinal extent of the beam is increased above ~1 cm in FOV_z. For CBCT systems, the scatter-to-primary ratio (SPR) incident on the detector is often well in excess of 100% – i.e., the majority of photons incident on the detector are scatter, not primary. MDCT systems up to 64 detector rows (FOV_z ~3.2 cm) have correspondingly lower SPR. MDCT systems with 320 rows, however, experience a similar level of SPR as CBCT and therefore incorporate a highly optimized post-patient collimation (2D focused anti-scatter grid) and scatter correction algorithms to minimize scatter artifacts and maintain soft-tissue contrast resolution.

Imaging Performance: Artifacts Associated with the Detector

CBCT systems based on FPDs contend with a variety of detector characteristics that can introduce artifacts in 3D image reconstructions. Instability (drift) in detector dark current motivates frequent dark/offset correction for FPDs – e.g., collection of dark frames prior to each CBCT scan. Higher levels of image lag (~1–5%) for FPDs can also introduce lag artifacts associated with residual signal from one projection view to the next. A typical example of lag artifact is evident in the "radar artifact" visible as a crescent-shaped non-uniformity in elliptical sites (e.g., head or pelvis) as the FPD signal varies strongly from unattenuated views to heavily attenuated views.

MDCT detectors, on the other hand, tend to exhibit lower levels of image lag and drift in dark current or gain such that they are addressed via regular air calibrations. Highly optimized, modular detector technology combined with low-noise readout electronics with greater digitization bit depth than CBCT tends to minimize such artifacts.

Imaging Performance: Artifacts Associated with the System Geometry

Cone-beam projection data acquisition from a circular source-detector orbit involves incomplete sampling of the 3D object, in accordance with Tuy's condition [49]. Specifically, circular orbit CBCT sampling exhibits a "null cone" about the longitudinal (f_z) Fourier domain axis, with the angular extent of the null cone varying with spatial position in the 3D object – viz., with angular extent equal to the angle subtended between the central axial plane and a particular position within the 3D reconstruction. Therefore, only the central axial plane is fully sampled, and locations "above" or "below" the central plane (i.e., at $z \neq 0$) are subject to undersampling effects that increase with $|z|$. The effect manifests as "cone-beam artifacts" evident as shading and streaks about structures with high f_z spatial-frequency content – e.g., a horizontal edge, as might be found at a joint space oriented parallel to the plane of the source-detector orbit.

In principle, cone-beam artifacts are present for both CBCT systems and MDCT systems with a large cone angle (e.g., MDCT systems with 320 detector rows), since they arise simply as a result of incomplete sampling from a circular geometry. Helical sampling helps to mitigate the effect – as does any orbit that breaks from the axial plane, such as circle-and-line, sinusoid-on-cylinder, or double-semicircle orbits. Such orbits improve f_z sampling, reducing the null cone and mitigating cone-beam artifacts. A helical orbit introduces potential sampling effects of its own, of course, and depending on the choice of helical pitch, undersampling effects and reconstruction errors ("windmill artifacts") may be observed as streaks about high-frequency structures.

Imaging Performance: Artifacts Associated with the Subject

Biases in projection data introduced by the subject include x-ray scatter and beam hardening (as mentioned above – increasing with larger subjects with greater attenuation) as well as photon starvation (strong attenuation resulting in near-zero detector signal). The term "metal artifact" associated with highly attenuating implants, for example, refers to a combination of effects, each of which introduces bias and/or data inconsistency – namely, strong attenuation, strong shift in the transmitted polyenergetic x-ray spectrum, and high-frequency content subject to undersampling effects. Both CBCT and MDCT systems are subject to such effects.

A potentially strong source of image degradation in CBCT is patient motion during the scan – including cardiac motion, respiratory motion, peristalsis, or involuntary drift or jitter. Motion artifacts appear as blur or distortion of anatomical structures and can confound visibility of both low-contrast soft-tissue and high-contrast bone detail. For CBCT systems with long scan times (e.g., >10 s), motion effects can be especially pronounced and present a major source of image degradation.

Such effects are much less severe in MDCT for two reasons. First, the MDCT gantry rotation speed is typically very fast (e.g., ~0.2–0.3 s per rotation) so that the motion within a single rotation is minimal. Secondly, for helical MDCT, the volumetric image is acquired via fast longitudinal motion of the table, and data inconsistencies associated with patient motion tend not to reinforce within angularly sampled, backprojected data in a particular axial plane. That is not to say that MDCT is immune to patient motion artifacts – e.g., "mushroom" artifact sometimes observed in coronal planes at the dome of the diaphragm – but tend to be much less severe than in slow-scan CBCT, which enjoys neither of these two advantages.

Dosimetry

Methods for CBCT dosimetry have been described by Daly et al. [50] and Fahrig et al. [10]. Recognizing that CBCT systems typically operate without table motion, commonly employ short-scan protocols, and have a volumetric beam typically >10 cm in FOV_z, CBCT dosimetry varies somewhat from the methodology established early in the development of axial CT. Specifically, CBCT dosimetry tends to employ a small volume (e.g., 0.6 cc) Farmer ionization chamber to measure the dose (air kerma) at the center and four cardinal peripheral locations in a 16 cm diameter acrylic cylinder. The "point" dose measured at the center (D_o) and periphery (D_p) are combined in 1/3 and 2/3 proportion, respectively, to yield the "weighted" dose (D_w), analogous to $CTDI_w$ or $CTDI_{vol}$ in MDCT. For CBCT scan protocols with orbital extent less than 360° (common for C-arms), the weighted-dose D_w is estimated by 1/3 of D_o plus 2/3 of the *average* D_p measured over the four cardinal peripheral locations.

Clinical Applications

The scope of clinical applications for CBCT and MDCT is vast and is touched upon in numerous instances above. The broad variety in form and function is evident in the diversity of CBCT scanner platforms shown in Fig. 2.2.

There is considerable overlap in application space for these modalities, but a coarse distinction can be stated: CBCT finds primary application in image-guided procedures (e.g., IGRT, image-guided surgery, and interventional radiology) and secondarily in emerging areas of diagnostic specialties (e.g., CBCT of the breast or extremities) – with dental/ENT CBCT being the clear exception; conversely, MDCT is primarily applied in diagnostic radiology and is, in fact, a major frontline workhorse for diagnostic imaging in areas ranging from trauma to cancer and secondarily in image-guided interventions (e.g., portable MDCT systems or CT-on-rails for image-guided procedures). This distinction in primary areas of application is far from absolute, and it is likely to diminish altogether as CBCT systems improve in image quality and, conversely, MDCT systems increase in diversity of form and flexibility.

Fig. 2.2 Example CBCT systems. (**a**) CBCT for dental/ENT imaging (Carestream). (**b**) Mobile CBCT for image-guided ENT surgery. (Xoran; photo courtesy of Dr. R. Labadie, Vanderbilt University). (**c**) CBCT for imaging of musculoskeletal/orthopedic extremities (foot, ankle, knee, hand, wrist, or elbow; Carestream). (**d**) Prototype U-arm for CBCT of the head [32]. (**e**) Mobile C-arm CBCT for image-guided surgery (Siemens Healthineers). (**f**) Early prototype CBCT breast scanner. (Photograph courtesy of Dr. J. Boone, University of California – Davis). (**g**) Robotic C-arm for CBCT in interventional radiology (Siemens Healthineers). (**h**) CBCT on a radiotherapy linac for IGRT (Elekta Oncology)

Regulations and Accreditation

MDCT is subject to well-recognized regulatory requirements and accreditation standards established by the American Board of Radiology (ABR). As a result, MDCT systems are subject to well-codified standards of dosimetry, quality assurance (QA), quality control (QC), accreditation, indications for meaningful use, and charge codes.

At the time of this writing, the regulatory requirements, accreditation standards, and charge codes associated with CBCT are nascent by comparison. Recent years have seen emerging effort to establish accreditation standards appropriate to CBCT dental/ENT systems, and one may expect similar efforts in other areas of CBCT clinical application. Example efforts include ongoing Task Group activity by the American Association of Physicists in Medicine (AAPM) – e.g., TG #238 on CBCT-capable C-arms – and IEC MT39 on standards for dental CBCT.

Emerging Topics and Ongoing Research

The areas of ongoing research are as diverse as the topics delineated above, aiming to improve image quality, reduce radiation dose, and extend the application of CBCT (and MDCT) to new applications and capabilities.

Novel X-Ray Sources Research on the development of new x-ray sources for CBCT include multi-source systems. One example is the three-source system incorporated in the Carestream Onsight system for extremity imaging to extend FOV_z and reduce cone-beam sampling effects [33]. Another includes research by Boone et al. to develop breast CBCT systems featuring ~10 x-ray sources [51]. Note that these multi-source systems involve a distribution of sources along the z-axis (cf., sources distributed azimuthally as in dual-source MDCT).

New Scan Protocols Another area of active research involves modulation of the x-ray beam to reduce dose and enable region-of-interest CBCT and MDCT. Modulation of kV and mA is fairly standard. Incorporation of a bowtie filter is standard in MDCT, but less frequent in CBCT [52]. Recent research aims to develop dynamic modulation of the beam during the scan using actuated bowtie filters, multi-leaf partially attenuating collimators, and multi-aperture devices [53].

Novel Detectors and Readout Modes Development of improved x-ray detectors is similarly an active area of research. In CBCT, novel detectors aim to reduce electronic noise, increase dynamic range, and increase spatial resolution. Strategies include development of dynamic gain readout modes and new detector architectures based on CMOS [25] and architectures giving on-pixel amplification [54]. The incorporation of photon-counting detectors (PCDs) has emerged in MDCT, and photon counting with large-area detectors suitable to CBCT is an active area of research [55].

Improved Reconstruction Algorithms Novel algorithms for 3D image reconstruction present a major area of ongoing research and development. By ~2010, MBIR had emerged in mainstream use in MDCT for diagnostic radiology, offering the potential for dose reduction [56]. Parallel activities extended MBIR methods to improve image quality and/or reduce dose in CBCT [43]. Recently, deep learning-based reconstruction methods are emerging to give comparable performance to MBIR with potential advantages of reduced runtime and computational complexity [57]. Such methods, along with adaptive local filtering [58], are likely to contribute to ongoing advances in CBCT and MDCT performance.

New Scanner Platforms and Applications We can anticipate a diversification of the form and application of MDCT systems in the decade ahead not unlike the diverse spectrum of CBCT systems that emerged in their original genesis in dental, C-arm, and IGRT systems. We are already seeing such diversification of MDCT in systems such as the Brainlab Airo. As commented upon below, a diversification of form and function in MDCT with an eye to specialty diagnostic applications, image-guided interventions, and point-of-care imaging signals a vibrant space of MDCT technology development.

Accordingly, one can anticipate adaptation of MDCT to specialty systems specifically designed for diagnostic specialties, adapting to forms beyond the iconic fixed ring gantry that is so iconic of diagnostic radiology. Such specialty areas presented fertile ground for dental CBCT since ~2000 and more recent systems for breast CBCT [59–61], musculoskeletal/orthopedic CBCT [15, 62–64] and even imaging of head trauma [32, 65]. Each of these areas broke new ground in extending certain advantages of CBCT in various diagnostic specialties, but the CBCT systems that emerged carried the challenges of CBCT image quality. We can anticipate the development of specialized MDCT systems to answer the call, evidenced by systems such as MDCT breast scanner [66] and dedicated MDCT head scanner [67].

Similarly, one can anticipate the adaptation of MDCT to forms better suited to image-guided interventional procedures than the conventional fixed ring gantry. Of course, direct translation of a diagnostic CT scanner into the interventional theater has been done, but such direct translation carries a lack of integration with interventional workflow that has presented bottlenecks in patient transfer and operating room (OR) logistics. New MDCT systems specially designed for interventional procedures beckon. Key examples are the BodyTom and Brainlab Airo.

Such diversification in the form and function of CBCT and MDCT systems further emphasizes the need to knowledgeably delineate their distinctions and commonalities as surveyed in the sections above. The ruling factors of cost, workflow, and performance will weigh in what is likely to be an exciting space of technology development – and a challenge to regulatory and accreditation requirements.

Conclusions

The sections above surveyed the distinctions and commonalities among CBCT and MDCT systems, and at each turn, we found areas of overlap.

CBCT is MDCT insofar as it incorporates a detector with multiple rows. On a personal note, I recall the outbreak of the Slice Wars in the early 2000s – marveling at the excitement within the CT community of 4-, 8-, 16-, and 64-slice detectors – and a strange sense as I worked to implement volumetric imaging with a FPD involving 1024 rows. I was not entirely sure if we were onto something big, or if we were beyond the realm of what could be reasonably asked of a large-area detector and 3D image reconstruction algorithm; however, I suspected the former. Moreover, CBCT systems based on XRIIs were already emerging. Many had proven analytically the incompleteness of cone beam sampling: the bumblebee would not fly. It did.

MDCT is CBCT insofar as it employs an x-ray beam that encompasses appreciable extent in the longitudinal (z) direction. On another personal note, I recall first seeing the 256-slice MDCT detector incorporated in the Toshiba Aquilion scanner and its subsequent release as a 320-slice MDCT scanner in diagnostic radiology – and marveling at what I perceived as a quantum leap beyond the performance of FPDs that I knew well in the development of CBCT systems. I thought the technologies of MDCT and CBCT may soon completely converge – and in accordance with the distinctions and commonalities traced in the preceding sections, they had indeed converged at least in principle. Interestingly, as described above, the technological embodiments and clinical applications of MDCT and CBCT remained fairly distinct in the following decades.

The sections above quickly surveyed these distinctions and commonalities in terms of system geometry, choice of x-ray source and detector, image acquisition and reconstruction techniques, imaging modes, image quality, artifacts, dosimetry, clinical applications, and regulatory considerations. So what did we learn?

Interestingly, we see that the term "cone beam" is not only insufficient in precisely distinguishing the modalities, it is somewhat of a misnomer to begin with. Perhaps the distinction between flat and curved detectors is a salient distinction for the time being at least, suggesting a meaningful dichotomy between "flat-detector CT" (FDCT) and "curved detector CT" (CDCT). While that dichotomy may be important with respect to the weighting term in the filtered backprojection algorithm and the design of post-patient collimator, it is not likely to be a durable distinction, and we can anticipate "curved" FPDs on flexible substrates [68]. Neither is the distinction between open-geometry (e.g., C-arms) and closed-bore (e.g., donut) systems meaningful – as FPD-CBCT systems abound in closed geometries as well (e.g., Medtronic O-arm and Varian Halcyon), and we might even envision open-geometry MDCT systems in the future for interventional procedures.

There is, therefore, no absolute distinction according to the survey provided above. Nonetheless, the survey hopefully provides sufficient perspective for the reader interested in these modalities to "know it when she/he sees it" – at least within the current state of the art: CBCT systems with FPDs in open-geometry platforms widespread in image-guidance (and filling specialty niche in diagnostics) and MDCT systems with curved detectors in closed geometry scanners as the backbone of diagnostic radiology (and filling specialty niche applications in image-guided interventions). Alternatively, this chapter may at least equip the reader to speak knowledgeably within the context of technologies between which a simple distinction does not exist.

As a final note, one might anticipate that any remaining confusion between these modalities in their form, application, and capabilities may be temporary and the need to differentiate between the two may melt away. The distinctions in form and application may diminish altogether in years ahead. Advances in x-ray sources, detector technologies, and 3D image reconstruction will advance the performance of volumetric tomography systems (or more generally, "volumetric imaging" systems, since the "tomo" prefix itself is somewhat of a misnomer) and enable application across the spectrum of diagnostic and image-guided procedures described above.

The distinction may be lost from a technological standpoint, leaving the question of whether regulatory administration of volumetric imaging systems will keep up in a manner that properly reflects the spectrum of technologies.

References

1. Hsieh J. Computed tomography: principles, design, artifacts, and recent advances. Computed tomography: principles, design, artifacts, and recent advances. 2nd ed. Bellingham: SPIE; 2015.
2. Buzug TM. Computed tomography: from photon statistics to modern cone-beam CT. Berlin: Springer; 2008.
3. Shaw C, editor. Cone beam computed tomography imaging in medical diagnosis and therapy. Boca Raton: CRC; 2014.
4. Brock KK, editor. Image processing in radiation therapy imaging in medical diagnosis and therapy. Boca Raton: CRC; 2016.
5. Zhou SK, editor. Handbook of medical image computing and computer assisted intervention. Boca Raton: CRC; 2019.
6. Siewerdsen JH, Moseley DJ, Burch S, Bisland SK, Bogaards A, Wilson BC, et al. Volume CT with a flat-panel detector on a mobile, isocentric C-arm: pre-clinical investigation in guidance of minimally invasive surgery. Med Phys [Internet]. 2005 [cited 2014 May 27];32(1):241–254. Available from: http://www.ncbi.nlm.nih.gov/pubmed/15719975.
7. Jaffray DA, Siewerdsen JH, Wong JW, Martinez AA. Flat-panel cone-beam computed tomography for image-guided radiation therapy. Int J Radiat Oncol Biol Phys [Internet]. 2002 [cited 2014 May 27];53(5):1337–1349. Available from: http://www.ncbi.nlm.nih.gov/pubmed/12128137.
8. Uneri A, Zhang X, Stayman JW, Helm P, Osgood GM, Theodore N, et al. Advanced image registration and reconstruction using the O-arm system: dose reduction, image quality, and guidance using known-component models. In: Webster RJ, Fei B, editors. SPIE medical imaging. Houston: SPIE; 2018. p. 43.
9. Siewerdsen JH. Cone-beam CT with a flat-panel detector: from image science to image-guided surgery. Nucl Instrum Methods Phys Res A [Internet]. 2011 [cited 2014 May 27];648(S1):S241–S250. Available from: http://www.pubmedcentral.nih.gov/articlerender.fcgi?artid=3429946&tool=pmcentrez&rendertype=abstract.
10. Fahrig R, Dixon R, Payne T, Morin RL, Ganguly A, Strobel N. Dose and image quality for a cone-beam C-arm CT system. Med Phys [Internet]. 2006;33(12):4541–50. Available from: http://www.ncbi.nlm.nih.gov/pubmed/17278805.
11. Lauzier PT, Tang J, Chen G-H. Time-resolved cardiac interventional cone-beam CT reconstruction from fully truncated projections using the prior image constrained compressed sensing (PICCS) algorithm. Phys Med Biol [Internet]. 2012;57(9):2461–76. Available from: http://stacks.iop.org/0031-9155/57/i=9/a=2461?key=crossref.9bc9545e6024e4a480c719410b4ec593.
12. Pauwels R, Araki K, Siewerdsen JH, Thongvigitmanee SS. Technical aspects of dental CBCT: state of the art. Dentomaxillofacial Radiol [Internet]. 2015;44(1):20140224. Available from: http://www.birpublications.org/doi/10.1259/dmfr.20140224.
13. Xu J, Reh DD, Carey JP, Mahesh M, Siewerdsen JH. Technical assessment of a cone-beam CT scanner for otolaryngology imaging: image quality, dose, and technique protocols. Med Phys [Internet]. 2012 [cited 2014 May 27];39(8):4932–4942. Available from: http://www.ncbi.nlm.nih.gov/pubmed/22894419.
14. Boone JM, Kwan ALC, Yang K, Burkett GW, Lindfors KK, Nelson TR. Computed tomography for imaging the Breast. J Mammary Gland Biol Neoplasia [Internet]. 2006;11(2):103–11. Available from: http://link.springer.com/10.1007/s10911-006-9017-1.
15. Carrino JA, Al Muhit A, Zbijewski W, Thawait GK, Stayman JW, Packard N, et al. Dedicated cone-beam CT system for extremity imaging. Radiology [Internet]. 2014 Mar [cited 2014 May 27];270(3):816–824. Available from: http://www.ncbi.nlm.nih.gov/pubmed/24475803.
16. Feldkamp LA, Davis LC, Kress JW. Practical cone-beam algorithm. J Opt Soc Am A [Internet]. 1984;1(6):612. Available from: https://www.osapublishing.org/abstract.cfm?URI=josaa-1-6-612.
17. Uneri A, Zhang X, Yi T, Stayman JW, Helm PA, Theodore N, et al. Image quality and dose characteristics for an O-arm intraoperative imaging system with model-based image reconstruction. Med Phys [Internet]. 2018;45(11):4857–68. Available from: https://onlinelibrary.wiley.com/doi/abs/10.1002/mp.13167.
18. Liang JZ, La Riviere PJ, El Fakhri G, Glick SJ, Siewerdsen J. Guest editorial low-dose CT: what has been done, and what challenges remain? IEEE Trans Med Imaging [Internet]. 2017;36(12):2409–16. Available from: http://ieeexplore.ieee.org/document/8125482/.
19. Stayman JW, Dang H, Ding Y, Siewerdsen JH. PIRPLE: a penalized-likelihood framework for incorporation of prior images in CT reconstruction. Phys Med Biol [Internet]. 2013 [cited 2014 Nov 18];58(21):7563–7582. Available from: http://www.pubmedcentral.nih.gov/articlerender.fcgi?artid=3868341&tool=pmcentrez&rendertype=abstract.
20. Gang GJ, Stayman JW, Ehtiati T, Siewerdsen JH. Task-driven image acquisition and reconstruction in cone-beam CT. Phys Med Biol [Internet]. 2015;60(8):3129–50. Available from: http://stacks.iop.org/0031-9155/60/i=8/a=3129?key=crossref.408e80cb449d4c28561d7a6c7f5688c8.

21. Tilley S, Siewerdsen JH, Stayman JW. Model-based iterative reconstruction for flat-panel cone-beam CT with focal spot blur, detector blur, and correlated noise. Phys Med Biol [Internet]. 2016;61(1):296–319. Available from: http://stacks.iop.org/0031-9155/61/i=1/a=296?key=crossref.4796deaf6827d354399470d1f41a47dc.
22. Heiland M, Schulze D, Adam G, Schmelzle R. 3D-imaging of the facial skeleton with an isocentric mobile C-arm system (Siremobil Iso-C 3D). Dentomaxillofacial Radiol [Internet]. 2003;32(1):21–5. Available from: http://www.birpublications.org/doi/10.1259/dmfr/80391180.
23. Zhang J, Weir V, Fajardo L, Lin J, Hsiung H, Ritenour ER. Dosimetric characterization of a cone-beam O-arm imaging system. J Xray Sci Technol [Internet]. 2009;17(4):305–17. Available from: http://www.ncbi.nlm.nih.gov/pubmed/19923687.
24. Ritschl L, Kuntz J, Fleischmann C, Kachelrieß M. The rotate-plus-shift C-arm trajectory. Part I. complete data with less than 180° rotation. Med Phys [Internet]. 2016 12;43(5):2295–2302. Available from: http://doi.wiley.com/10.1118/1.4944785.
25. Sheth NM, Zbijewski W, Jacobson MW, Abiola G, Kleinszig G, Vogt S, et al. Mobile C-arm with a CMOS detector: technical assessment of fluoroscopy and cone-beam CT imaging performance. Med Phys [Internet]. 2018;45(12):5420–36. Available from: https://onlinelibrary.wiley.com/doi/abs/10.1002/mp.13244.
26. Chen B, Ning R. Cone-beam volume CT breast imaging: feasibility study. Med Phys [Internet]. 2002;29(5):755–70. Available from: http://doi.wiley.com/10.1118/1.1461843.
27. Jaffray DA, Siewerdsen JH. Cone-beam computed tomography with a flat-panel imager: initial performance characterization. Med Phys [Internet]. 2000 [cited 2014 May 27];27(6):1311–1323. Available from: http://www.ncbi.nlm.nih.gov/pubmed/10902561.
28. Fahrig R, Holdsworth DW. Three-dimensional computed tomographic reconstruction using a C-arm mounted XRII: image-based correction of gantry motion nonidealities. Med Phys [Internet]. 2000;27(1):30–8. Available from: http://doi.wiley.com/10.1118/1.598854.
29. Arai Y, Honda K, Iwai K, Shinoda K. Practical model "3DX" of limited cone-beam X-ray CT for dental use. Int Congr Ser [Internet]. 2001;1230:713–8. Available from: http://linkinghub.elsevier.com/retrieve/pii/S0531513101001194.
30. Hu H, He HD, Foley WD, Fox SH. Four multidetector-row helical CT: image quality and volume coverage speed. Radiology [Internet]. 2000;215(1):55–62. Available from: http://pubs.rsna.org/doi/10.1148/radiology.215.1.r00ap3755.
31. Pan X, Siewerdsen J, La Riviere PJ, Kalender WA. Anniversary paper: development of x-ray computed tomography: the role of medical physics and AAPM from the 1970s to present. Med Phys [Internet]. 2008;35(8):3728–39. Available from: http://doi.wiley.com/10.1118/1.2952653.
32. Xu J, Sisniega A, Zbijewski W, Dang H, Stayman JW, Mow M, et al. Technical assessment of a prototype cone-beam CT system for imaging of acute intracranial hemorrhage. Med Phys. 2016;43(10):5745.
33. Gang GJ, Zbijewski W, Mahesh M, Thawait G, Packard N, Yorkston J, et al. Image quality and dose for a multisource cone-beam CT extremity scanner. Med Phys [Internet]. 2018;45(1):144–55. Available from: http://www.ncbi.nlm.nih.gov/pubmed/29121409.
34. Flohr TG, McCollough CH, Bruder H, Petersilka M, Gruber K, Süβ C, et al. First performance evaluation of a dual-source CT (DSCT) system. Eur Radiol [Internet]. 2006;16(2):256–68. Available from: http://link.springer.com/10.1007/s00330-005-2919-2.
35. Siewerdsen JH, Jaffray DA. Cone-beam computed tomography with a flat-panel imager: magnitude and effects of x-ray scatter. Med Phys [Internet]. 2001;28(2):220–31. Available from: http://doi.wiley.com/10.1118/1.1339879.
36. Schafer S, Stayman JW, Zbijewski W, Schmidgunst C, Kleinszig G, Siewerdsen JH. Antiscatter grids in mobile C-arm cone-beam CT: effect on image quality and dose. Med Phys [Internet]. 2012 [cited 2014 May 27];39(1):153–159. Available from: http://www.pubmedcentral.nih.gov/articlerender.fcgi?artid=3261054&tool=pmcentrez&rendertype=abstract.
37. Siewerdsen JH, Moseley DJ, Bakhtiar B, Richard S, Jaffray DA. The influence of antiscatter grids on soft-tissue detectability in cone-beam computed tomography with flat-panel detectors. Med Phys [Internet]. 2004. [cited 2014 May 27];31;(12):3506–20.. Available from: http://www.ncbi.nlm.nih.gov/pubmed/15651634
38. Sisniega A, Zbijewski W, Badal A, Kyprianou IS, Stayman JW, Vaquero JJ, et al. Monte Carlo study of the effects of system geometry and antiscatter grids on cone-beam CT scatter distributions. Med Phys [Internet]. 2013 [cited 2014 May 27];40(5):051915. Available from: http://www.pubmedcentral.nih.gov/articlerender.fcgi?artid=3651212&tool=pmcentrez&rendertype=abstract.
39. Weir VJ, Zhang J, Bruner AP. Dosimetric characterization and image quality evaluation of the AIRO mobile CT scanner. J Xray Sci Technol [Internet]. 2015;23(3):373–81. Available from: http://www.medra.org/servlet/aliasResolver?alias=iospress&doi=10.3233/XST-150496.
40. Barsa P, Frőhlich R, Beneš V, Suchomel P. Intraoperative portable CT-scanner based spinal navigation – a feasibility and safety study. Acta Neurochir (Wien) [Internet]. 2014;156(9):1807–12. Available from: http://link.springer.com/10.1007/s00701-014-2184-8.
41. Katsevich A. Analysis of an exact inversion algorithm for spiral cone-beam CT. Phys Med Biol [Internet]. 2002;47(15):302. Available from: http://stacks.iop.org/0031-9155/47/i=15/a=302?key=crossref.a6eb76dffee2c2ce17372b064074320b.

42. Siewerdsen JH, Daly MJ, Bachar G, Moseley DJ, Bootsma G, Brock KK, et al. Multimode C-arm fluoroscopy, tomosynthesis, and cone-beam CT for image-guided interventions: from proof of principle to patient protocols. In: Hsieh J, Flynn MJ, editors. Proc SPIE [Internet]. 2007 [cited 2014 Jul 17];6510:65101A–65101A–11. Available from: http://proceedings.spiedigitallibrary.org/proceeding.aspx?articleid=1299299.
43. Wang AS, Stayman JW, Otake Y, Kleinszig G, Vogt S, Gallia GL, et al. Soft-tissue imaging with C-arm cone-beam CT using statistical reconstruction. Phys Med Biol [Internet]. 2014 [cited 2014 May 27];59(4):1005–1026. Available from: http://www.pubmedcentral.nih.gov/articlerender.fcgi?artid=4046706&tool=pmcentrez&rendertype=abstract.
44. Prakash P, Zbijewski W, Gang GJ, Ding Y, Stayman JW, Yorkston J, et al. Task-based modeling and optimization of a cone-beam CT scanner for musculoskeletal imaging. Med Phys [Internet]. 2011 [cited 2014 May 27];38(10):5612–5629. Available from: http://www.pubmedcentral.nih.gov/articlerender.fcgi?artid=3208412&tool=pmcentrez&rendertype=abstract.
45. Dang H, Stayman JW, Sisniega A, Xu J, Zbijewski W, Wang X, et al. Statistical reconstruction for cone-beam CT with a post-artifact-correction noise model: application to high-quality head imaging. Phys Med Biol [Internet]. 2015 [cited 2015 Aug 18];60(16):6153–6175. Available from: http://www.ncbi.nlm.nih.gov/pubmed/26225912.
46. Dang H, Stayman JW, Xu J, Zbijewski W, Sisniega A, Mow M, et al. Task-based statistical image reconstruction for high-quality cone-beam CT. Phys Med Biol. 2017;62(22):8693–719.
47. Dang H, Stayman JW, Sisniega A, Zbijewski W, Xu J, Wang X, et al. Multi-resolution statistical image reconstruction for mitigation of truncation effects: application to cone-beam CT of the head. Phys Med Biol. 2017;62(2):539–59.
48. Sisniega A, Zbijewski W, Xu J, Dang H, Stayman JW, Yorkston J, et al. High-fidelity artifact correction for cone-beam CT imaging of the brain. Phys Med Biol [Internet]. 2015 [cited 2015 Jan 29];60(4):1415–1439. Available from: http://www.ncbi.nlm.nih.gov/pubmed/25611041.
49. Defrise M, Clack R. A cone-beam reconstruction algorithm using shift-variant filtering and cone-beam backprojection. IEEE Trans Med Imaging [Internet]. 1994;13(1):186–95.. Available from: http://ieeexplore.ieee.org/document/276157/
50. Daly MJ, Siewerdsen JH, Moseley DJ, Jaffray DA, Irish JC. Intraoperative cone-beam CT for guidance of head and neck surgery: assessment of dose and image quality using a C-arm prototype. Med Phys [Internet]. 2006 [cited 2014 May 27];33(10):3767–3780. Available from: http://www.ncbi.nlm.nih.gov/pubmed/17089842.
51. Hernandez AM, Schwoebel P, Boone JM, Becker A. Multisource x-ray system for artifact reduction in dedicated breast CT. In: Krupinski EA, editor. 14th International Workshop on Breast Imaging (IWBI 2018) [Internet]. SPIE; 2018. p. 19. Available from: https://www.spiedigitallibrary.org/conference-proceedings-of-spie/10718/2317846/Multisource-x-ray-system-for-artifact-reduction-in-dedicated-breast/10.1117/12.2317846.full.
52. Xu J. Evaluation of detector readout gain mode and bowtie filters for cone-beam CT imaging of the head. Phys Med Biol [Internet]. 2016;61(16):5973–5992(20). Available from: http://www.ncbi.nlm.nih.gov/pubmed/?term=Evaluation+of+detector+readout+gain+mode+and+bowtie+filters+for+cone-beam+CT+imaging+of+the+head.
53. Stayman JW. Fluence-field modulated x-ray CT using multiple aperture devices. Proc Soc Photo Opt Instrum Eng [Internet]. 2016. Available from: http://proceedings.spiedigitallibrary.org/proceeding.aspx?articleid=2506547.
54. El-Mohri Y, Antonuk LE, Koniczek M, Zhao Q, Li Y, Street RA, et al. Active pixel imagers incorporating pixel-level amplifiers based on polycrystalline-silicon thin-film transistors. Med Phys [Internet]. 2009;36(7):3340–55. Available from: http://doi.wiley.com/10.1118/1.3116364.
55. Stavro J, Goldan AH, Zhao W. SWAD: inherent photon counting performance of amorphous selenium multi-well avalanche detector. In: Kontos D, Flohr TG, Lo JY, editors. 2016. p. 97833Q. Available from: http://proceedings.spiedigitallibrary.org/proceeding.aspx?doi=10.1117/12.2217248.
56. Pickhardt PJ, Lubner MG, Kim DH, Tang J, Ruma JA, del Rio AM, et al. Abdominal CT with model-based iterative reconstruction (MBIR): initial results of a prospective trial comparing ultralow-dose with standard-dose imaging. Am J Roentgenol [Internet]. 2012;199(6):1266–74. Available from: http://www.ajronline.org/doi/10.2214/AJR.12.9382.
57. Chen H, Zhang Y, Kalra MK, Lin F, Chen Y, Liao P, et al. Low-dose CT with a residual encoder-decoder convolutional neural network. IEEE Trans Med Imaging [Internet]. 2017;36(12):2524–35. Available from: https://ieeexplore.ieee.org/document/7947200/.
58. Li Z, Yu L, Trzasko JD, Lake DS, Blezek DJ, Fletcher JG, et al. Adaptive nonlocal means filtering based on local noise level for CT denoising. Med Phys [Internet]. 2013 Dec 31;41(1):011908. Available from: http://doi.wiley.com/10.1118/1.4851635.
59. Lindfors KK, Boone JM, Nelson TR, Yang K, Kwan ALC, Miller DF. Dedicated breast CT: Initial clinical experience. Radiology [Internet]. 2008;246(3):725–33. Available from: http://pubs.rsna.org/doi/10.1148/radiol.2463070410.
60. Kwan ALC, Boone JM, Yang K, Huang S-Y. Evaluation of the spatial resolution characteristics of a cone-beam breast CT scanner. Med Phys [Internet]. 2006;34(1):275–81. Available from: http://doi.wiley.com/10.1118/1.2400830.
61. Zhao B, Zhang X, Cai W, Conover D, Ning R. Cone beam breast CT with multiplanar and three dimensional visualization in differentiating

breast masses compared with mammography. Eur J Radiol [Internet]. 2015;84(1):48–53. Available from: https://linkinghub.elsevier.com/retrieve/pii/S0720048X14002903.

62. Thawait GK, Demehri S, AlMuhit A, Zbijweski W, Yorkston J, Del Grande F, et al. Extremity cone-beam CT for evaluation of medial tibiofemoral osteoarthritis: initial experience in imaging of the weight-bearing and non-weight-bearing knee. Eur J Radiol [Internet]. 2015 [cited 2015 Nov 19]; Available from: http://www.ncbi.nlm.nih.gov/pubmed/26388464.
63. Demehri S, Muhit A, Zbijewski W, Stayman JW, Yorkston J, Packard N, et al. Assessment of image quality in soft tissue and bone visualization tasks for a dedicated extremity cone-beam CT system. Eur Radiol [Internet]. 2015 25(6):1742–1751 [cited 2015 Apr 17]; Available from: http://www.ncbi.nlm.nih.gov/pubmed/25599933.
64. de Cesar NC, Schon LC, Thawait GK, da Fonseca LF, Chinanuvathana A, Zbijewski WB, et al. Flexible adult acquired flatfoot deformity. J Bone Jt Surg [Internet]. 2017;99(18):e98. Available from: http://insights.ovid.com/crossref?an=00004623-201709200-00015.
65. Sisniega A, Xu J, Dang H, Zbijewski W, Stayman JW, Mow M, et al. In: Flohr TG, Lo JY, Gilat Schmidt T, editors. Development and clinical translation of a cone-beam CT scanner for high-quality imaging of intracranial hemorrhage. Orlando: SPIE; 2017. p. 101320K.
66. Kalender WA, Kolditz D, Steiding C, Ruth V, Lück F, Rößler A-C, et al. Technical feasibility proof for high-resolution low-dose photon-counting CT of the breast. Eur Radiol [Internet]. 2017;27(3):1081–6. Available from: http://link.springer.com/10.1007/s00330-016-4459-3.
67. John S, Stock S, Cerejo R, Uchino K, Winners S, Russman A, et al. Brain imaging using Mobile CT: current status and future prospects. J Neuroimaging [Internet]. 2016;26(1):5–15. Available from: http://doi.wiley.com/10.1111/jon.12319.
68. Siewerdsen JH, Sisniega A, Zbijewski W, Wu P, Stayman JW, Koliatsos VE, et al. Image quality, scatter, and dose in compact CBCT systems with flat and curved detectors. In: Chen G-H, Lo JY, Gilat Schmidt T, editors. Medical imaging 2018: physics of medical imaging [internet]. Orlando: SPIE; 2018. p. 163. Available from: https://www.spiedigitallibrary.org/conference-proceedings-of-spie/10573/2293872/Image-quality-scatter-and-dose-in-compact-CBCT-systems-with/10.1117/12.2293872.full.